THE JOURNAL OF PHYSICAL CHEMISTRY Letters

Letter

Cite This: J. Phys. Chem. Lett. 2019, 10, 7965−7969

pubs.acs.org/JPCL

Doping Iron in $CsPbBr_3$ Perovskite Nanocrystals for Efficient and Product Selective CO_2 Reduction

Sanjib Shyamal, Sumit Kumar Dutta, and Narayan Pradhan*

School of Materials Sciences, Indian Association for the Cultivation of Science, Kolkata 700032, India

Supporting Information

ABSTRACT: Lead halide perovskite nanocrystals have recently emerged as an efficient optical material for light harvesting. While these have been extensively studied for obtaining bright emissions, their use as catalysts for enhancing the rate of chemical reactions has been explored little. Considering their importance in catalysis, herein, Fe(II)-doped $CsPbBr_3$ perovskite nanocrystals have been explored for photocatalytic reduction of CO_2. In comparison to undoped $CsPbBr_3$, doped nanocrystals showed enhanced catalytic activity and also predominantly led to evolution of CH_4 instead of CO. The observation of a reverse trend of predominated CH_4 evolution in doped nanocrystals rather than CO observed for undoped nanocrystals was correlated to the adsorption/desorption energy of respective products established theoretically earlier. This selective evolution of major products on doping remained unique and also a step forward for understanding more regarding light to chemical energy conversions using perovskite nanocrystals.

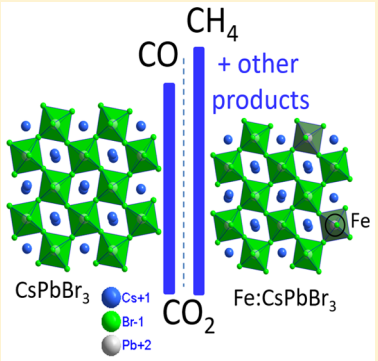

Perovskite nanocrystals have emerged as one of the most efficient light-harvesting materials in current research.[1−7] For light to light energy conversion, these have been extensively studied and as high as near unity photoluminescence quantum yields in different colors have been established.[5,8−14] However, because they are efficient light-absorbing materials, their utilization in light to chemical energy transformation is limited.[15−17] Major obstacles of these nanocrystals are their sensitivity towards polar environments and the strong recombination possibility of the photogenerated charge carriers.[3,18,19] Hence, unlike chalcogenide quantum dots, implementations of these nanocrystals in catalysis have been less explored. From the literature reports, it is revealed that methylammonium lead iodide ($MAPbI_3$) was used for the first time as a photocatalyst for the generation of hydrogen (H_2) from HI solution.[15] Soon thereafter, several groups extensively studied stable $CsPbBr_3$ perovskite nanostructures for photocatalytic CO_2 reduction.[16,19−21] Creating heterojunctions with highly conductive material [e.g., $CsPbBr_3$/graphene quantum dots (QDs), g-C_3N_4, and Pd nanosheets], carrier recombination possibilities were reduced and efficiencies of the catalytic activities of these materials were enhanced.[16,19,20,22] Again, upon tuning of the size and composition of the $CsPbBr_3$ perovskite nanocrystals, the productivity was also greatly enhanced.[21] Beyond the reduction, controlling the selectivity of products from CO_2 reduction is also important, and using $CsPbBr_3$ nanocrystals as photocatalysts, this aspect of controlling the products is also limited.[19]

Recently, Tang et al. theoretically predicted the adsorption energies of different products in various forms of metal-doped $CsPbBr_3$.[23] Inspired by this report in which Co and Fe were proposed as ideal dopants to predominantly produce methane, herein, Fe(II)-doped $CsPbBr_3$ nanocrystals were synthesized and explored for photocatalytic reduction of CO_2. With 3% Fe(II) doping (with respect to Pb), the obtained doped $CsPbBr_3$ showed selectively CH_4 as the dominant product where the undoped $CsPbBr_3$ led to CO as the major product. In addition, the catalytic performance for the doped nanocrystals was also observed to be enhanced. The efficient photocatalysis is also supported by measuring the transient current and comparing the catalytic activities in several controlled reactions. Postcatalysis samples were also vividly characterized, and the presence of Fe as the key for twisting the catalytic path for these nanocrystal catalysts was established. To the best of our knowledge, this is a unique report in which catalysts were used without any additional carrier transportation material or heterostructures.

For the synthesis of $CsPbBr_3$ nanocrystals, the reported literature method[1] was adopted, and for doping, an optimized 25% of the Fe(II) precursor (with respect to Pb) was introduced into the reaction system before injection of the Cs(I) precursor. The doping of Fe(II) was expected to replace Fe(II) in the position of Pb(II) in the lattice. Atomic models for the doped and undoped $CsPbBr_3$ nanocrystals are shown in Figure 1. The selectivity of products CH_4 and CO from doped and undoped nanocrystals is schematically also shown in this figure, which was experimentally found and discussed below.

Figure 2a shows the absorption and photoluminescence (PL) spectra of as-synthesized hexane dispersed undoped and doped $CsPbBr_3$ nanocrystals. Their spectral nature and

Received: October 28, 2019
Accepted: December 2, 2019
Published: December 2, 2019

DOI: 10.1021/acs.jpclett.9b03176
J. Phys. Chem. Lett. 2019, 10, 7965−7969

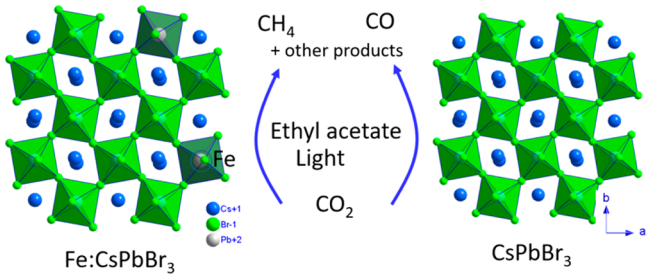

Figure 1. Schematic presentation of Fe-doped $CsPbBr_3$ and undoped $CsPbBr_3$ nanocrystal photocatalysts leading to CH_4 and CO as the major products, respectively, in photocatalytic CO_2 reduction reaction.

positions remained similar and as expected from reported $CsPbBr_3$ nanocrystals.[1,3] Figure 2b presents the transmission electron microscopic (TEM) image of undoped $CsPbBr_3$ nanocrystals, and Figure 2c shows the TEM image of Fe(II)-doped nanocrystals. The size of these nanocrystals remained 12−15 nm, and the dispersity also remained identical. However, with a larger amount of Fe(II), the disparity remained wider (Figure S1) and the catalytic activities decreased (discussed below).

These as-synthesized $CsPbBr_3$ and Fe(II)-doped $CsPbBr_3$ nanocrystals were further explored for photocatalytic CO_2 reduction in an ethyl acetate/water medium[20] with an incident light intensity of 150 mW cm^{-2}. The ethyl acetate medium was chosen because of its mild polarity and the high solubility of CO_2, and this had also been optimized in a previous report.[16] Details of the experimental procedure are provided in the Supporting Information. The photocatalytic performances of undoped, Fe(II)-doped $CsPbBr_3$, and only Fe(II) acetate salt as control reaction are presented in Figure 3. Plots of the time-dependent evolution of the products CH_4 and CO using these catalysts are provided in panels a and b of Figure 3, respectively. Importantly, it has been observed that there are differences in the product selectivity of the undoped and doped photocatalysts toward CO_2 reduction. The major products CO (4.6 μmol g^{-1} h^{-1}) and CH_4 (1.9 μmol g^{-1} h^{-1}) were obtained for undoped $CsPbBr_3$ nanocrystals, which were also shown in previous reports (Table S1).[17,19,20] However, doped nanocrystals predominantly formed CH_4 in comparison to CO. In optimized Fe(II) doping (loading of 25% with respect to Pb), the maximum amount of CH_4 (6.1 μmol g^{-1} h^{-1}) evolved over CO (3.2 μmol g^{-1} h^{-1}). Moreover, the addition of an excess of Fe was harmful to the photocatalytic performance, resulting in decreasing the amount of products (shown in Figure S2). The corresponding energy dispersive spectra (EDS) and elemental compositions are shown in Figure S3. In addition, to observe the impact of Fe(II) acetate salt without nanocrystals, the control reaction was also carried out in an ethyl acetate/water medium during catalysis; however, the reactions were seen to be much slower compared to the presence of nanocrystal catalysts. Another possible reaction by mixing Fe(II) acetate salts with $CsPbBr_3$ nanocrystals without doping was also measured under similar conditions; however, the rate of reduction was observed to be slower (Figure S4). Via combination of all of these results, including control reaction without Fe(II) and nanocrystals, the evolved CH_4 and CO gases are shown quantitatively in Figure 3c. From all of these observations, the catalytic activity for selective production of CH_4 was observed for Fe(II)-doped $CsPbBr_3$ nanocrystals. Furthermore, to confirm the generated CH_4 and CO gases produced from photocatalytic CO_2 reduction, the control experiment was also carried out without CO_2 under the same condition. The result (Figure S5) showed an insignificant amount of CO that might be from partial photo-oxidation of ethyl acetate or other trace organic contamination, but no CH_4 was traced.

Furthermore, to understand the ability to transport photogenerated charge carriers, these nanostructures were explored for photoelectrochemical (PEC) measurements. These measurements were carried out in a 0.1 M solution of tetrabutylammonium hexafluorophosphate ($TBAPF_6$) in ethyl acetate under 150 mW cm^{-2} solar light illumination. Figure 3d represents the chronoamperometric $I-t$ plot at −0.4 V versus Ag/AgCl of the undoped, Fe(II)-doped $CsPbBr_3$, and only Fe(II) acetate salt. From the plot, it was evident that the photocurrent was repeatable with light on−off cycles. The maximum PEC photocurrent density of −120 μA cm^{-2} was observed for Fe(II)-doped $CsPbBr_3$ (25% Fe loading with respect to Pb) nanocrystals that was 3.15 times that of undoped nanocrystals (38 μA cm^{-2}). Figure 3e presents the chronoamperometric $I-t$ plots of the photoelectrodes using different percentages of Fe(II)-doped $CsPbBr_3$ nanocrystals and measured at −0.4 V versus Ag/AgCl. The observed photocurrent density gradually increased from 0% to 25% and then decreased with a higher doping percentage. This change in the trend was also found in good agreement with the photocatalytic CO_2 reduction efficiency (Figure S2). PEC

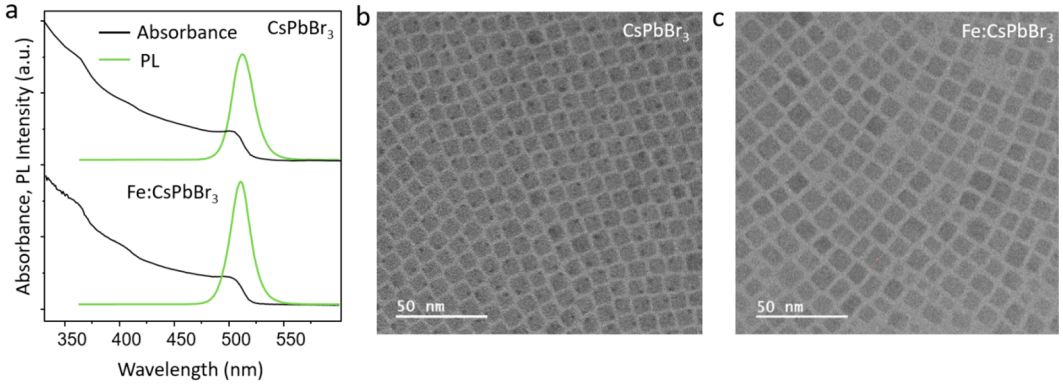

Figure 2. (a) Absorption and photoluminescence (PL) spectra of as-synthesized $CsPbBr_3$ and Fe(II)-doped $CsPbBr_3$ nanocrystal photocatalysts. The excitation wavelength was 350 nm. TEM images of (b) $CsPbBr_3$ and (c) Fe(II)-doped $CsPbBr_3$ nanocrystals.

DOI: 10.1021/acs.jpclett.9b03176
J. Phys. Chem. Lett. 2019, 10, 7965−7969

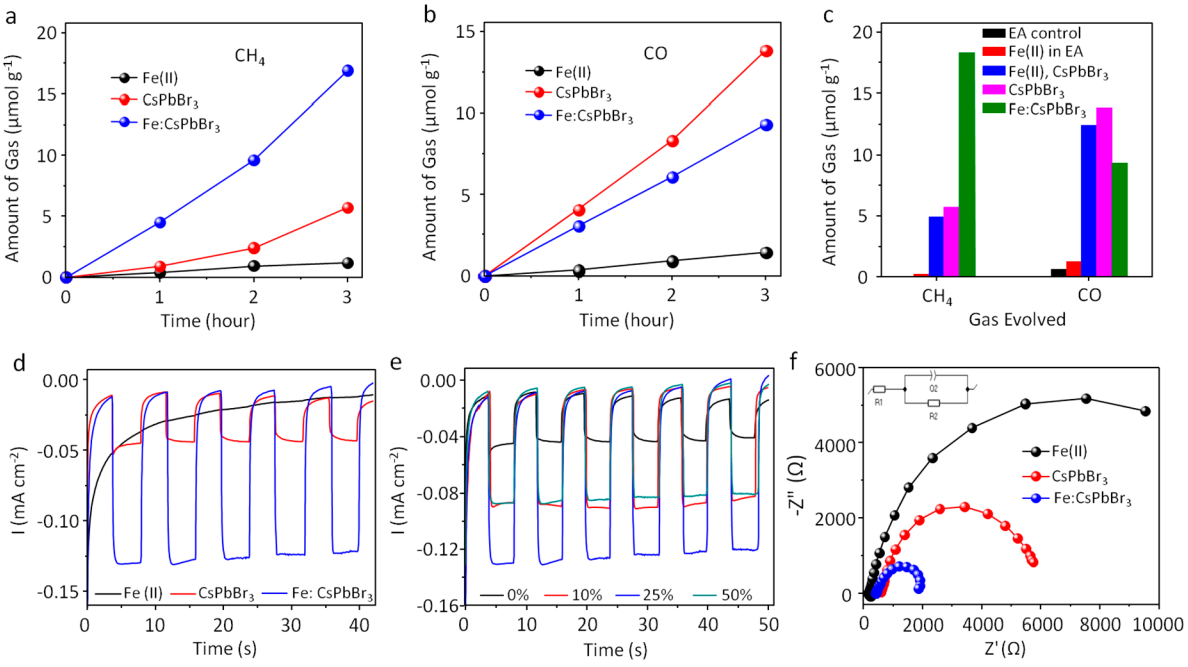

Figure 3. Quantitative evolutions of (a) CH_4 gas and (b) CO gas from $CsPbBr_3$, Fe(II)-doped $CsPbBr_3$ nanocrystals as photocatalysts, and the control reaction using only Fe(II) acetate salt during the process of photocatalytic reduction of CO_2 over time. (c) Bar diagram showing relative ratios of CH_4 and CO produced using addition of Fe(II) acetate to $CsPbBr_3$, $CsPbBr_3$, and Fe(II)-doped $CsPbBr_3$, only Fe(II) acetate without $CsPbBr_3$ and the control reaction without any additive. (d) Transient photocurrent response of photoelectrodes having $CsPbBr_3$, Fe(II)-doped $CsPbBr_3$ nanocrystals, and the control reaction using only Fe(II) acetate salt. (e) Transient photocurrent response of photoelectrodes having doped $CsPbBr_3$ prepared with different Fe(II) loading with respect to Pb. (f) Nyquist plots of $CsPbBr_3$ nanocrystals, Fe(II)-doped $CsPbBr_3$ nanocrystals, and only Fe(II)acetate salt. The inset shows the electrochemical circuit used for calculation.

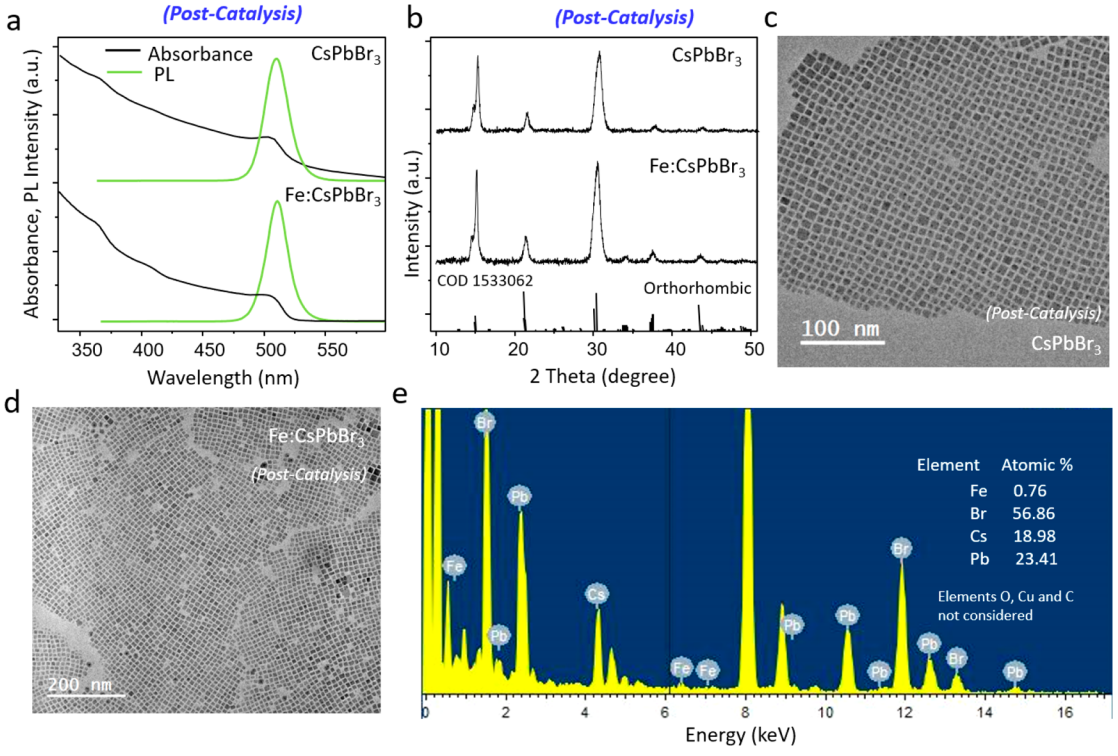

Figure 4. (a) Absorption and PL spectra of postcatalysis $CsPbBr_3$ and Fe(II)-doped $CsPbBr_3$ nanocrystals. (b) Powder X-ray diffraction patterns of postcatalysis undoped and doped $CsPbBr_3$ nanocrystals. (c) TEM image of postcatalysis $CsPbBr_3$ nanocrystals. (d) TEM image of postcatalysis Fe(II)-doped $CsPbBr_3$ nanocrystals. (e) EDS spectra of postcatalysis Fe(II)-doped $CsPbBr_3$ nanocrystals. The excited wavelength for the PL spectra measurement was 350 nm.

DOI: 10.1021/acs.jpclett.9b03176
J. Phys. Chem. Lett. 2019, 10, 7965−7969

impedance spectra were measured to detect the charge transport behavior of prepared electrodes and are shown in Figure 3f. The Nyquist plot suggested the obvious decrease in the charge transfer resistance (R_{ct}) for the Fe(II)-doped $CsPbBr_3$ photoelectrode in comparison to undoped and the controlled Fe(II) electrodes. Using the simple R-C circuit model,[24] the fitted values are listed in Table S2. Hence, all of the PEC data were observed in good agreement with the photocatalytic CO_2 reduction activity, and doped nanocrystals were superior.

In addition, to observe the sustainability of these nanocrystals, postcatalysis samples were also analyzed. These nanocrystals in ethyl acetate were agglomerated and not properly soluble, and hence, these were precipitated with centrifugation and redispersed in hexane for optical measurements. Figure 4a presents the absorption and PL spectra of postcatalysis $CsPbBr_3$ and Fe(II)-doped $CsPbBr_3$ nanocrystals, and all of these retained almost the identical spectra. In some cases, scatterings were observed because of agglomeration, but upon dilution, clear spectra could be obtained. Figure 4b shows powder X-ray diffraction (XRD) patterns of both doped and undoped postcatalysis nanocrystals, and both retained the orthorhombic phase. Figure 4c shows the TEM image of postcatalysis $CsPbBr_3$, and Figure 4d shows that of Fe(II)-doped $CsPbBr_3$, which retained the cubic shape. In some places on the grid, we observed agglomerations (Figure S6) that were expected because of the poor solubility in polar ethyl acetate medium. Energy dispersive spectra (EDS) of Fe(II)-doped $CsPbBr_3$ after exposure for 3 h to light during photocatalysis and further with purification are shown in Figure 4e. The calculated Fe atomic percentage of 25% (with respect to Pb) loading during the preparation of doped nanocrystals retained only 0.76% within the nanocrystals after catalysis. The amount retained almost 3% Fe(II) with respect to Pb(II) in the perovskite nanocrystals.

From all of the results presented above, it could be confirmed here that Fe(II)-doped $CsPbBr_3$ perovskite nanocrystals acted as better catalysts and also performed selectivity in CO_2 to methane production. Even doping transition metal ions were extensively studied for stabilizing and enhancing photoluminescence intensity, increasing the photoresponse property, yielding dopant-induced new emission, etc.,[4,25−30] but this was not explored for photocatalytic CO_2 reduction. Hence, it became important for understanding the underlying mechanism of carrier transportation during photocatalysis. As stated above, Tang et al.[23] theoretically predicted the ability of such reduction using several metal ions. For the case of Fe(II) doping, the adsorption energy for CH_4 was reported to be more positive, indicating active CH_4 molecules once formed were faster desorbed from the catalyst surfaces. This enhanced the reaction in favor of methane production in Fe(II)-doped $CsPbBr_3$ and CO for undoped $CsPbBr_3$ nanocrystals. This desorption mechanism in the energy diagram is shown in Figure 5. However, while we tried the same reactions with Co(II), that was also predicted to be efficient dopant, but a poor catalytic performance was recorded (Figure S7). This might need modifications of the reaction procedure or a different catalytic strategy.

While the entire study was carried out using Fe(II) ions for doping, nanocrystals were also synthesized using Fe(III) precursor. Unfortunately, efficient doping could not be obtained under similar conditions and Fe could not be detected in purified nanocrystals (Figure S8). Hence, it could

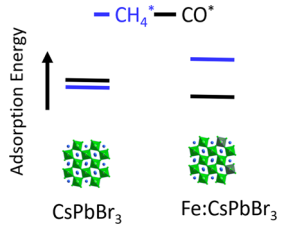

Figure 5. Schematic presentation of the energy diagram of adsorption of active CH_4 and CO molecules onto the surface of undoped and doped $CsPbBr_3$ nanocrystals.

be stated here that Fe(II) facilitated the doping forming octahedra like Pb(II) under our adopted reaction protocol.

In conclusion, Fe(II)-doped $CsPbBr_3$ nanocrystals as product selective and efficient photocatalysts for reduction of CO_2 are established. While undoped $CsPbBr_3$ led to CO as the major product, doping Fe(II) helped to evolve CH_4 as the predominated gas from photocatalytic reduction of CO_2. Unlike previous reports, these photocatalysts did not require any additional carrier transportation material or heterostructures. Transient current measurement also supported Fe(II)-doped nanocrystals as a better photoconductor and showed a superior photoresponse compared to that of its undoped counterpart. Carrying out several controlled reactions and analyzing the postcatalysis samples, we established that doping in $CsPbBr_3$ indeed enhanced the catalytic activities of these nanocrystals. These results with selective CH_4 and CO as major products for doped and undoped nanocrystals were further correlated with their adsorption and desorption abilities on the catalyst surfaces, which have been predicted theoretically.[23] To the best of our knowledge, these findings of product selectivity are new and would yield a wider understanding of the catalytic activities of these newly emerged perovskite nanomaterials.

■ ASSOCIATED CONTENT

Supporting Information

The Supporting Information is available free of charge at https://pubs.acs.org/doi/10.1021/acs.jpclett.9b03176.

Materials, methods, instrumentation, photoelectrochemical measurement procedure, photochemical CO_2 reduction procedure, EDS spectra, TEM images, gas chromatography data, chronoamperometry $I-t$ plot, comparison of literature reports, and table of electrochemical circuit parameters (PDF)

■ AUTHOR INFORMATION

Corresponding Author

*E-mail: camnp@iacs.res.in.

ORCID

Sanjib Shyamal: 0000-0002-7255-506X

Sumit Kumar Dutta: 0000-0002-9228-1916

Narayan Pradhan: 0000-0003-4646-8488

Notes

The authors declare no competing financial interest.

■ ACKNOWLEDGMENTS

SERB of India (EMR/2016/001795) is acknowledged for funding. S.K.D. acknowledges CSIR SPM for a fellowship.

DOI: 10.1021/acs.jpclett.9b03176
J. Phys. Chem. Lett. 2019, 10, 7965−7969

REFERENCES

(1) Protesescu, L.; Yakunin, S.; Bodnarchuk, M. I.; Krieg, F.; Caputo, R.; Hendon, C. H.; Yang, R. X.; Walsh, A.; Kovalenko, M. V. Nanocrystals of Cesium Lead Halide Perovskites ($CsPbX_3$, X = Cl, Br, and I): Novel Optoelectronic Materials Showing Bright Emission with Wide Color Gamut. *Nano Lett.* **2015**, *15*, 3692−3696.

(2) Akkerman, Q. A.; Rainò, G.; Kovalenko, M. V.; Manna, L. Genesis, Challenges and Opportunities for Colloidal Lead Halide Perovskite Nanocrystals. *Nat. Mater.* **2018**, *17*, 394−405.

(3) Shamsi, J.; Urban, A. S.; Imran, M.; De Trizio, L.; Manna, L. Metal Halide Perovskite Nanocrystals: Synthesis, Post-Synthesis Modifications, and Their Optical Properties. *Chem. Rev.* **2019**, *119*, 3296−3348.

(4) Zhou, Y.; Chen, J.; Bakr, O. M.; Sun, H.-T. Metal-Doped Lead Halide Perovskites: Synthesis, Properties, and Optoelectronic Applications. *Chem. Mater.* **2018**, *30*, 6589−6613.

(5) Zheng, X.; Hou, Y.; Sun, H.-T.; Mohammed, O. F.; Sargent, E. H.; Bakr, O. M. Reducing Defects in Halide Perovskite Nanocrystals for Light-Emitting Applications. *J. Phys. Chem. Lett.* **2019**, *10*, 2629−2640.

(6) Meinardi, F.; Akkerman, Q. A.; Bruni, F.; Park, S.; Mauri, M.; Dang, Z.; Manna, L.; Brovelli, S. Doped Halide Perovskite Nanocrystals for Reabsorption-Free Luminescent Solar Concentrators. *ACS Energy Lett.* **2017**, *2*, 2368−2377.

(7) Zhang, Q.; Yin, Y. All-Inorganic Metal Halide Perovskite Nanocrystals: Opportunities and Challenges. *ACS Cent. Sci.* **2018**, *4*, 668−679.

(8) Dutta, A.; Behera, R. K.; Pal, P.; Baitalik, S.; Pradhan, N. Near-Unity Photoluminescence Quantum Efficiency for All $CsPbX_3$ (X = Cl, Br, and I) Perovskite Nanocrystals: A Generic Synthesis Approach. *Angew. Chem., Int. Ed.* **2019**, *58*, 5552−5556.

(9) Mondal, N.; De, A.; Samanta, A. Achieving Near-Unity Photoluminescence Efficiency for Blue-Violet-Emitting Perovskite Nanocrystals. *ACS Energy Lett.* **2019**, *4*, 32−39.

(10) Yong, Z.-J.; Guo, S.-Q.; Ma, J.-P.; Zhang, J.-Y.; Li, Z.-Y.; Chen, Y.-M.; Zhang, B.-B.; Zhou, Y.; Shu, J.; Gu, J.-L.; et al. Doping-Enhanced Short-Range Order of Perovskite Nanocrystals for Near-Unity Violet Luminescence Quantum Yield. *J. Am. Chem. Soc.* **2018**, *140*, 9942−9951.

(11) Ahmed, T.; Seth, S.; Samanta, A. Boosting the Photoluminescence of $CsPbX_3$ (X = Cl, Br, I) Perovskite Nanocrystals Covering a Wide Wavelength Range by Postsynthetic Treatment with Tetrafluoroborate Salts. *Chem. Mater.* **2018**, *30*, 3633−3637.

(12) Pradhan, N. Tips and Twists in Making High Photoluminescence Quantum Yield Perovskite Nanocrystals. *ACS Energy Lett.* **2019**, *4*, 1634−1638.

(13) Liu, F.; Zhang, Y.; Ding, C.; Kobayashi, S.; Izuishi, T.; Nakazawa, N.; Toyoda, T.; Ohta, T.; Hayase, S.; Minemoto, T.; et al. Highly Luminescent Phase-Stable $CsPbI_3$ Perovskite Quantum Dots Achieving Near 100% Absolute Photoluminescence Quantum Yield. *ACS Nano* **2017**, *11*, 10373−10383.

(14) Bohn, B. J.; Tong, Y.; Gramlich, M.; Lai, M. L.; Döblinger, M.; Wang, K.; Hoye, R. L. Z.; Müller-Buschbaum, P.; Stranks, S. D.; Urban, A. S.; et al. Boosting Tunable Blue Luminescence of Halide Perovskite Nanoplatelets through Postsynthetic Surface Trap Repair. *Nano Lett.* **2018**, *18*, 5231−5238.

(15) Park, S.; Chang, W. J.; Lee, C. W.; Park, S.; Ahn, H.-Y.; Nam, K. T. Photocatalytic Hydrogen Generation from Hydriodic Acid using Methylammonium Lead Iodide in Dynamic Equilibrium with Aqueous Solution. *Nat. Energy* **2017**, *2*, 16185.

(16) Xu, Y.-F.; Yang, M.-Z.; Chen, B.-X.; Wang, X.-D.; Chen, H.-Y.; Kuang, D.-B.; Su, C.-Y. A $CsPbBr_3$ Perovskite Quantum Dot/Graphene Oxide Composite for Photocatalytic CO_2 Reduction. *J. Am. Chem. Soc.* **2017**, *139*, 5660−5663.

(17) Kong, Z.-C.; Liao, J.-F.; Dong, Y.-J.; Xu, Y.-F.; Chen, H.-Y.; Kuang, D.-B.; Su, C.-Y. Core@Shell $CsPbBr_3$@Zeolitic Imidazolate Framework Nanocomposite for Efficient Photocatalytic CO_2 Reduction. *ACS Energy Lett.* **2018**, *3*, 2656−2662.

(18) Behera, R. K.; Das Adhikari, S.; Dutta, S. K.; Dutta, A.; Pradhan, N. Blue-Emitting $CsPbCl_3$ Nanocrystals: Impact of Surface Passivation for Unprecedented Enhancement and Loss of Optical Emission. *J. Phys. Chem. Lett.* **2018**, *9*, 6884−6891.

(19) Xu, Y.-F.; Yang, M.-Z.; Chen, H.-Y.; Liao, J.-F.; Wang, X.-D.; Kuang, D.-B. Enhanced Solar-Driven Gaseous CO_2 Conversion by $CsPbBr_3$ Nanocrystal/Pd Nanosheet Schottky-Junction Photocatalyst. *ACS Appl. Energy Mater.* **2018**, *1*, 5083−5089.

(20) Ou, M.; Tu, W.; Yin, S.; Xing, W.; Wu, S.; Wang, H.; Wan, S.; Zhong, Q.; Xu, R. Amino-Assisted Anchoring of $CsPbBr_3$ Perovskite Quantum Dots on Porous g-C_3N_4 for Enhanced Photocatalytic CO_2 Reduction. *Angew. Chem., Int. Ed.* **2018**, *57*, 13570−13574.

(21) Guo, S.-H.; Zhou, J.; Zhao, X.; Sun, C.-Y.; You, S.-Q.; Wang, X.-L.; Su, Z.-M. Enhanced CO_2Photoreduction via Tuning Halides in Perovskites. *J. Catal.* **2019**, *369*, 201−208.

(22) Pan, A.; Ma, X.; Huang, S.; Wu, Y.; Jia, M.; Shi, Y.; Liu, Y.; Wangyang, P.; He, L.; Liu, Y. $CsPbBr_3$ Perovskite Nanocrystal Grown on MXene Nanosheets for Enhanced Photoelectric Detection and Photocatalytic CO_2 Reduction. *J. Phys. Chem. Lett.* **2019**, *10*, 6590−6597.

(23) Tang, C.; Chen, C.; Xu, W.; Xu, L. Design of Doped Cesium Lead Halide Perovskite as a Photo-Catalytic CO_2 Reduction Catalyst. *J. Mater. Chem. A* **2019**, *7*, 6911−6919.

(24) Klahr, B.; Gimenez, S.; Fabregat-Santiago, F.; Hamann, T.; Bisquert, J. Water Oxidation at Hematite Photoelectrodes: The Role of Surface States. *J. Am. Chem. Soc.* **2012**, *134*, 4294−4302.

(25) Begum, R.; Parida, M. R.; Abdelhady, A. L.; Murali, B.; Alyami, N. M.; Ahmed, G. H.; Hedhili, M. N.; Bakr, O. M.; Mohammed, O. F. Engineering Interfacial Charge Transfer in $CsPbBr_3$ Perovskite Nanocrystals by Heterovalent Doping. *J. Am. Chem. Soc.* **2017**, *139*, 731−737.

(26) Swarnkar, A.; Mir, W. J.; Nag, A. Can B-Site Doping or Alloying Improve Thermal- and Phase-Stability of All-Inorganic $CsPbX_3$ (X = Cl, Br, I) Perovskites? *ACS Energy Lett.* **2018**, *3*, 286−289.

(27) Das Adhikari, S.; Guria, A. K.; Pradhan, N. Insights of Doping and the Photoluminescence Properties of Mn-Doped Perovskite Nanocrystals. *J. Phys. Chem. Lett.* **2019**, *10*, 2250−2257.

(28) Pan, G.; Bai, X.; Yang, D.; Chen, X.; Jing, P.; Qu, S.; Zhang, L.; Zhou, D.; Zhu, J.; Xu, W.; et al. Doping Lanthanide into Perovskite Nanocrystals: Highly Improved and Expanded Optical Properties. *Nano Lett.* **2017**, *17*, 8005−8011.

(29) Lu, M.; Zhang, X.; Bai, X.; Wu, H.; Shen, X.; Zhang, Y.; Zhang, W.; Zheng, W.; Song, H.; Yu, W. W.; et al. Spontaneous Silver Doping and Surface Passivation of $CsPbI_3$ Perovskite Active Layer Enable Light-Emitting Devices with an External Quantum Efficiency of 11.2%. *ACS Energy Lett.* **2018**, *3*, 1571−1577.

(30) Cheng, X.; Jing, L.; Yuan, Y.; Du, S.; Zhang, J.; Zhan, X.; Ding, J.; Yu, H.; Shi, G. Fe^{2+}/Fe^{3+} Doped into $MAPbCl_3$ Single Crystal: Impact on Crystal Growth and Optical and Photoelectronic Properties. *J. Phys. Chem. C* **2019**, *123*, 1669−1676.

DOI: 10.1021/acs.jpclett.9b03176
J. Phys. Chem. Lett. 2019, 10, 7965−7969